batteries

MDPI

Review

Photocuring in Lithium-Ion Battery Fabrication: Advances Towards Integrated Manufacturing

Zihao Li [1,*], Yanlong Li [1], Mengting Chen [1], Weishan Li [2,*] and Xiaoming Wei [1]

[1] School of Physics and Optoelectronics, State Key Laboratory of Luminescent Materials and Devices, Guangdong Engineering Technology Research and Development Center of Special Optical Fiber Materials and Devices, Guangdong Provincial Key Laboratory of Fiber Laser Materials and Applied Techniques, South China University of Technology, Guangzhou 510640, China; 202411088767@mail.scut.edu.cn (Y.L.); 202211087338@mail.scut.edu.cn (M.C.); xmwei@scut.edu.cn (X.W.)

[2] School of Chemistry, South China Normal University, Guangzhou 510006, China

* Correspondence: phlzh@scut.edu.cn (Z.L.); liwsh@scnu.edu.cn (W.L.)

Abstract

Photocuring, including photopolymerization and photocrosslinking, has emerged as a transformative manufacturing paradigm that enables the precise, rapid, and customizable fabrication of advanced battery components. This review first introduces the principles of photocuring and vat photopolymerization and their unique advantages of high process efficiency, non-contact fabrication, ambient-temperature processing, and robust interlayer bonding. It then systematically summarizes photocured battery components, involving electrolytes, membranes, anodes, and cathodes, highlighting their design strategies. This review examines the impact of photocured materials on the battery's properties, such as its conductivity, lithium-ion transference number, and mechanical strength, while examining how vat-photopolymerization-derived 3D architectures optimize ion transport and electrode–electrolyte integration. Finally, it discusses current challenges and future directions for photocuring-based battery manufacturing, emphasizing the need for specialized energy storage resins and scalable processes to bridge lab-scale innovations with industrial applications.

Keywords: photocuring; lithium-ion batteries; 3D printing; vat photopolymerization

Academic Editor: Yong-Joon Park

Received: 30 June 2025
Revised: 16 July 2025
Accepted: 21 July 2025
Published: 23 July 2025

Citation: Li, Z.; Li, Y.; Chen, M.; Li, W.; Wei, X. Photocuring in Lithium-Ion Battery Fabrication: Advances Towards Integrated Manufacturing. *Batteries* **2025**, *11*, 282. https://doi.org/10.3390/batteries11080282

1. Introduction

The rapid advancement of modern society has driven unprecedented demands for electrochemical energy sources, particularly in lithium-ion batteries (LIBs), which serve as the cornerstone for modern energy storage. With the global shift toward renewable energy and carbon neutrality, these rechargeable batteries are expected to deliver not only higher energy density and power density but also extended the cycle life, rapid charge/discharge capabilities, and adaptability to diverse application scenarios. Consumer electronics increasingly require lighter, thinner, flexible, and high-capacity power sources to match miniaturization trends. The electronics and electric vehicle industry requires batteries with lower weight and improved thermal management to address range anxiety and charging infrastructure limitations. Meanwhile, grid-scale energy storage systems necessitate cost-effective, long-lasting batteries that are capable of stabilizing intermittent renewable energy sources such as wind and solar. Emerging applications in the Internet of Things, smart sensors, and micro-/nano-devices further push the boundaries of battery

technology, requiring microscale power sources with high volumetric energy density and customizable geometries.

However, conventional battery manufacturing techniques face intrinsic limitations in meeting these multifaceted requirements. Established processes such as slurry casting, roll-to-roll electrode coating, and mechanical calendaring struggle to fabricate complex battery structures with geometrically optimized architectures such as 3D scaffolds, interdigitated arrays, or gradient porosity designs that could simultaneously enhance ion diffusion kinetics and active material utilization. The inherent trade-off between energy density and power density in traditional laminated or stacked electrode configurations remains unresolved, as thicker electrodes for higher energy storage inevitably prolong ion transport paths, increasing internal resistance. Customization for specialized applications, such as conformal batteries for irregularly shaped devices or microscale power sources, is unfeasible with conventional techniques. Furthermore, the multi-step nature of traditional production, involving slurry drying, compression, assembly, electrolyte filling, and degassing, introduces inefficiencies and quality control challenges. The growing adoption of next-generation battery chemistries, including silicon anodes, sulfur cathodes, and solid-state electrolytes, exacerbates these limitations, as conventional methods lack the precision to handle volume-expansion-sensitive materials or brittle ceramic solid electrolytes.

In this context, batteries with 3D architectures have emerged as a transformative paradigm for battery fabrication [1,2]. Additive manufacturing, colloquially referred to as 3D printing, is an important means of fabricating 3D batteries; it eliminates the need for molds or dies, enabling the direct digital-to-physical translation of complex geometries through layer-by-layer material deposition. Moreover, 3D printing facilitates the customization of internal architectures and overcomes the shape limitations of conventional batteries, which enhances their electrochemical as well as mechanical properties and enables high-level integration with other components, as well as customized designs tailored to specific spatial requirements [3,4]. Its core advantage of a high degree of freedom aligns perfectly with the evolving demands of advanced manufacturing. The convergence of 3D printing with battery technologies addresses three critical industrial needs: performance optimization through structural engineering, rapid prototyping through short-cycle iterations, and economical small-batch customization [5]. In practical terms, 3D printing's single-step fabrication capabilities reduce production timelines while allowing for the simultaneous integration of multiple components in a single print job.

Among the diverse 3D printing techniques explored for battery manufacturing, three primary categories have emerged as prominent due to their unique capabilities: material extrusion, material jetting, and vat photopolymerization [6,7]. Material extrusion encompasses methods such as fused deposition modeling and direct ink writing, which excel in depositing bulk materials for relatively large batteries. Material jetting, including inkjet printing and aerosol jet printing, offers precision in depositing functional materials without polymer binders. Vat photopolymerization stands out for its unparalleled resolution and capacity to fabricate intricate geometries [8]. Other methods, such as powder bed fusion, binder jetting, and sheet lamination, are also under investigation but face challenges in balancing electrochemical functionality with structural complexity.

Vat photopolymerization (VPP) is a group of light-based maskless 3D printing technologies that mainly utilize ultraviolet light to selectively cure photosensitive resins layer by layer, solidifying the precise structures dictated by digital models [9]. The process involves iterative steps of light exposure and platform repositioning, enabling the creation of high-resolution structures with submicron features.

Stereolithography (SLA), digital light processing (DLP), and two-photon lithography (TPL) are three prominent VPP technologies that are widely applied in advanced manufac-

turing [10,11], as shown in Figure 1. The characteristic parameters of the VPP techniques are listed in Table 1. Among them, SLA is one of the earliest and most established photopolymerization techniques [12], which utilizes a focused UV laser to selectively scan the surface layer of resin, which photopolymerizes at precise locations to solidify each layer. This point-by-point approach enables high-resolution printing and excellent surface finish.

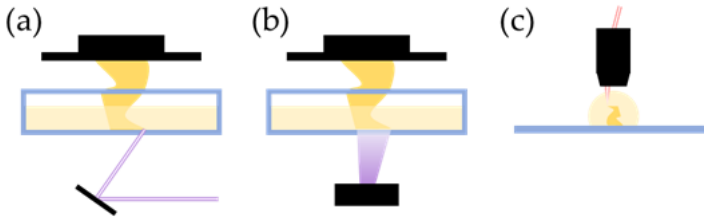

Figure 1. Schematic illustration of three vat photopolymerization techniques. (**a**) Stereolithography, (**b**) digital light processing, and (**c**) two-photon lithography.

DLP employs a digital micromirror device (DMD) to project entire layers of patterns simultaneously, enabling the rapid curing of complete resin layers [13,14]. The absence of sequential curing and uneven scanning speed in DLP ensures uniform polymerization across each layer. The layer-wise solidification significantly enhances printing efficiency, minimizes residual intralayer stress, and reduces sensitivity to resin flowability and light scattering; it therefore allows DLP to support a broader range of materials [15].

TPL leverages nonlinear two-photon absorption induced by tightly focused ultrafast lasers to trigger photochemical reactions within a highly localized focal volume of resin [16]. This approach enables sub-100 nm resolution, surpassing the diffraction limits of conventional UV-based methods [17]. Not only does TPL requiring more sophisticated optical systems but, unlike SLA and DLP, TPL curing occurs within the resin's interior, which places higher demands on the resin's optical properties such as transmittance [18].

Table 1. Typical characteristic parameters of VPP techniques [19–22].

	Maximum Printing Speed (mm^3/h)	Horizontal Resolution (μm)	Layer Thickness (μm)
SLA	~10^5	1–50	10–200
DLP	~10^6	10–50	1–100
TPL	~10^4	0.1–1	0.1–5

Collectively, these technologies offer complementary capabilities: SLA balances resolution and material adaptability for medium-scale functional parts, while DLP sacrifices a small amount of accuracy because of the limitation of the pixels of the DMD screen [23]. Though niche, TPL dominates scenarios demanding nanoscale features, albeit at the cost of speed. The choice among them depends on specific requirements such as resolution, material compatibility, production scale, and cost considerations. While TPL demonstrates unparalleled potential in microbattery fabrication, it remains noteworthy that it is the sole method not yet directly applied to battery component manufacturing among the three compared technologies.

Recent advancements have extended VPP to battery fabrication, which provides the following unparalleled advantages:

(1) VPP can achieve spatial resolutions far exceeding other 3D printing methods [24]. The featured high precision enables it to fabricate microscale battery structures and microbatteries [25]. Furthermore, the technology delivers outstanding surface quality with submicron-level roughness [26], minimizing inter-track and interlayer gaps.

(2) VPP uniquely enables the fabrication of complex 3D battery architectures. Unlike material jetting techniques that are limited to thin 2D deposits, or material extrusion methods that are restricted by nozzle dimensions and toolpaths, VPP enables the fabrication of complex geometries, including hollow cavities, cantilevered features, overhanging elements, interpenetrating networks, and structures embedded within or beneath light-permeable substrates, which empowers the creation of optimized electrode and electrolyte designs where tailored porosity and the maximized surface area directly enhance ion transport kinetics and electrochemical performance.
(3) VPP can achieve exceptional interlayer bonding through photopolymerization and photocrosslinking, forming robust covalent bonds between successive layers of both identical and dissimilar materials. Unlike physically stacked layers in fused filament fabrication or selective laser sintering, both of which are prone to delamination under mechanical or electrochemical stress, VPP's chemical bonding ensures the seamless integration of battery components at the molecular level. This results in structurally monolithic batteries, which are critical for streamlining the fabrication process and minimizing interfacial resistance in battery electrodes and electrolytes.
(4) VPP is a nozzle-free approach that additionally avoids common reliability issues associated with extrusion techniques, such as nozzle clogging and material dragging when processing particle-loaded inks or high-viscosity suspensions [27].

VPP also encounters several key inherent challenges. The production of 2D electrodes has achieved high efficiency, with slurry casting reaching 600–1800 m/h and electrostatic spray deposition at 6–12 m/h [28]. While photocuring is compatible with roll-to-roll processes [29], VPP techniques remain far from industrial battery production, as the point-scanning mechanism in SLA and TPP leads to slow processing speeds; increasing the throughput requires increasing light power [30]. Additionally, resin-based structures suffer from limited mechanical strength, causing deformation and deviations from the intended digital model. Polymerization shrinkage in acrylate-based resins results in 2–14% volumetric shrinkage [31], while residual interlayer stresses from constrained curing layers cause detachment and warping. Furthermore, some materials require post-processing such as debinding and sintering, leading to even greater shrinkage.

In terms of cost, VPP equipment is typically priced between the least expensive material extrusion and the most expensive material jetting technologies [32]. In terms of operational costs, VPP needs more expensive functional photocurable resins and higher light-source-related energy and maintenance expenses [33] compared to the low-cost material extrusion with its mature hardware and consumables system; however, it eliminates the need for the expensive, short-life nozzles used in material jetting. Nevertheless, the development of suitable resins for VPP still faces significant challenges, particularly as its material selection is constrained by multiple factors [34,35]. The resins require the precise optimization of photocuring, rheological, electrochemical, and mechanical properties, whereas conventional photosensitive resins lack electrochemical activity or charge transport capabilities. The excessive incorporation of such photoresists in battery fabrication would inevitably compromise electrochemical performance. Although the photocured materials can be converted via post-processing steps such as thermal debinding and sintering, which lend VPP the ability to fabricate more complex hybrid architectures [36], material adaptability remains the primary concern for applying VPP to battery manufacturing. Additionally, solvent orthogonality should also be considered when performing multilayer, multicomponent 3D printing to prevent interlayer dissolution. Compatibilities between photopolymers and other battery materials further raise the challenges in material screening.

Due to the limited availability of commercially developed energy-storage-specific resins, no reports have yet demonstrated the 3D printing of full lithium-ion batteries via

VPP, and the inherent limitations of VPP necessitate sustained research efforts. Recent years have witnessed a proliferation of studies focusing on photocurable battery components, with research on polymer electrolytes fabricated through photocuring dominating this field and driving significant advancements. Although 3D structural fabrication has not been the primary focus of these investigations, they have substantially advanced material selection and processing methodologies, while simultaneously establishing critical technological foundations that will accelerate the development of specialized energy-storage-specific resins.

Despite the growing interest in 3D-printed batteries, a systematic review of photocuring-based manufacturing for lithium-ion batteries and related systems remains scarce. This work focuses on the fabrication of key battery components, including electrodes, membranes, anodes, and cathodes, via photocuring techniques such as photopolymerization and photocrosslinking. Finally, the review discusses the implications of photocuring for both battery research and industrial applications.

2. Electrolytes

Solid polymer electrolytes (SPEs) have emerged as promising candidates for next-generation energy storage due to their enhanced safety and flexibility. However, conventional SPEs suffer from low room-temperature ionic conductivity, poor mechanical strength and poor interfacial stability. Photopolymerization offers a compelling solution, enabling rapid curing, precise control, and compatibility with scalable manufacturing. In contrast to current commercial polyolefin separators, which require uniform ~50% porosity to prevent uneven current distribution and lithium plating, photocured SPEs eliminate macropore dependency by enabling lithium-ion transport through polymer chain motion. Recent compositional and structural advances in SPEs have significantly improved their ion transport and mechanical properties. This review systematically summarizes material design strategies, structural optimization, and performance enhancements in photocured SPEs, while highlighting future directions for their practical implementation.

Common monomers in photocurable electrolytes include acrylates such as methyl methacrylate, as well as their specialized derivatives. Incorporating ether-oxygen containing PEG segments or cyano groups [37] into the monomer enhances ion transport capabilities, as seen in poly(ethylene glycol) methacrylate (PEGMA) or acrylonitrile; introducing additional hydroxyl groups improves adhesion and water retention properties [38,39], as exemplified by 2-hydroxyethyl acrylate (HEA); incorporating long alkyl chains increases the amorphous domain fraction and reduces ion migration barriers [40,41], as demonstrated by butyl acrylate (BA). Diacrylate and triacrylate such as polyethylene glycol diacrylate (PEGDA) and trimethylolpropane ethoxylate triacrylate (TMPETA) featuring multiple vinyl groups are often used as crosslinkers; they enable radical-initiated rapid crosslinking that enhances mechanical strength and preserves small electrolyte molecules. Additionally, the incorporated PEG segments shared by the crosslinkers facilitate ion transport. The solvent-free, room-temperature curing of these monomers and crosslinkers enables scalable fabrication without degrading thermosensitive components, in contrast to thermally cured electrolytes.

2.1. Influence of Plasticizers

Plasticizers increase polymer chain mobility by disrupting intermolecular forces, thereby enhancing the segmental motion of polymer chains (Figure 2). Owing to this property, they are frequently used in SPEs [42]. Among plasticizers, nitrile-based compounds featuring high bond energy and an elevated dielectric constant of their cyano groups demonstrate exceptional oxidative stability and superior lithium salt dissociation

capabilities. This enhances the room-temperature ionic conductivity of composite polymer electrolytes while maintaining their compatibility with high-voltage cathodes.

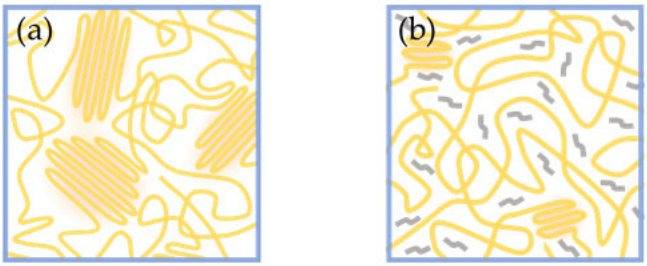

Figure 2. Schematic illustration of (**a**) the crystallinity of the polymer and (**b**) the effect of plasticization on the polymer.

In 2011, Ha et al. [43] pioneered the fabrication of a self-standing plastic crystal composite electrolyte (X-PCCE) by photocuring a crosslinked network of TMPETA. Succinonitrile (SN) served as the ionic conductor, where its dinitrile functional groups efficiently dissociated lithium bis(trifluoromethanesulfonyl)imide (LiTFSI) salt through strong polar interactions. This approach achieved a room-temperature ionic conductivity of 1.26 mS/cm and a tensile strength of 0.13 MPa—significantly higher than conventional PVdF-HFP-based electrolytes. It also demonstrated a wide electrochemical stability window, up to 5.0 V vs. Li^+/Li. He et al. [44] revealed the influence of prepolymer molecular weight on PEGDA/SN systems. It was found that PEGDA6000 with a high molecular weight will form a loose network with expanded chain-segmental free volume, increasing the elongation at break by one order of magnitude compared to X-PCCE. Concurrently, this structure provided enhanced migration pathways for SN, elevating the room-temperature ionic conductivity to 1.45 mS/cm. This breakthrough demonstrated that the combination of a high-MW polymer network and SN plasticization can overcome the traditional trade-off between mechanical strength and ionic conductivity.

Feng et al. [45] systematically compared the mechanism of dinitrile plasticizers with varying chain lengths: succinonitrile, glutaronitrile (GN), and adiponitrile (AN). GN exhibited the lowest melting point (−29 °C) due to its chain asymmetry, delivering optimal performance. In the 20/50/30 PEGDA/GLN/LiTFSI system, GN enabled an ionic conductivity of 2.3 mS/cm, which is double that of the SN-plasticized polymer electrolyte. Crucially, GN eliminated the low-temperature limitations of SN, maintaining an amorphous phase across a broad temperature range (−80 °C to 90 °C). This advance facilitates solid-state battery applications in extreme environments.

Qi et al. [46] proposed a rheology-tuning two-stage photopolymerization strategy to develop an electrolyte with synergistic ion-conductive channels. The study employs cyclic tetrahydrofurfuryl acrylate (THFA) as a functional monomer and incorporates plasticizer tetramethyl urea (TMU) to optimize ion transport. The former exhibits higher Li^+ binding energy than a conventional monomer with PEG side chains, while the latter's strong solvation capability effectively promotes lithium salt dissociation. The two-stage photocuring process first converts poly(ethylene glycol) methyl ether acrylate (PEGMEA)/THFA into a viscous syrup with shear-thinning properties, enabling compatibility with the blade-coating process. Subsequently, the rheology-tuned syrup is blended with PEGDA crosslinker, LiTFSI, and TMU and then coated onto a PET nonwoven substrate and cured, yielding the final electrolyte, which achieved a room-temperature ionic conductivity of 0.4 mS/cm and a lithium-ion transference number of 0.77. In electrochemical testing, Li//Li symmetric cells stably cycle for >900 h at 0.1 mA/cm^2, while $LiFePO_4$//Li full cells maintain 94.5% capacity retention after 200 cycles at 0.5C. This work provides an insight to resolve the bottleneck of

continuous coating production for photocured electrolytes. In the same year, Yuan et al. [47] impregnated a precursor solution composed of a photopolymerizable monomer PEGDA, LiTFSI, and the plasticizer SN into a commercial polyethylene (PE) separator. Subsequent photocrosslinking of PEGDA filled the PE pores, forming an ultrathin (16 μm) composite electrolyte. The resulting membrane exhibited a high room-temperature ionic conductivity of 0.11 mS/cm, a high elastic modulus of 6.37 MPa, and superior interfacial stability (Li//Li symmetric cells stably cycled for >1000 h at 0.1 mA/cm^2). These photocuring processes are readily compatible with roll-to-roll manufacturing, enabling scalable production.

In summary, as one of the general components in photocurable electrolytes, plasticizers also significantly affect cycling performance, as well as improving ionic conductivity and the rate performance. Fortunately, the optimal chain lengths for both conductivity and stability are coincident. Plasticizers with moderate chain lengths ensure uniform ionic channels and optimal performance, whereas short chains narrow the plastic crystal phase temperature window and promote phase separation via photopolymerization-induced crystallization, while long chains reduce plasticizing efficiency and ion dissociation capabilities. The lower molecular symmetry of the plasticizers helps to suppress crystallization. Strong Li^+ solvators (e.g., TMU) facilitate Li^+ dissociation while anchoring anions, curtailing side reactions, and preventing solid electrolyte interface (SEI) layer thickening; moreover, the continuous phase of TMU in the electrolyte, as compared to SCN's plastic–crystalline phase, homogenizes Li^+ flux and reduces interfacial gradients. Conversely, excessive plasticizer compromises mechanical strength and interfacial contact, while an overly low glass transition temperature risks high-temperature creep, undermining long-term stability.

2.2. SPEs with a PVDF-HFP Matrix

Traditional SPEs exhibit relatively low ionic conductivity due to their high crystallinity. To overcome this limitation, poly(vinylidene fluoride-co-hexafluoropropylene) (PVDF-HFP) emerged as a critical alternative. Its higher amorphous-phase content due to disrupted PVDF crystallinity by HFP segments reduces barriers to Li^+ diffusion, demonstrating improved room-temperature conductivity, while its superior electrochemical stability, arising from strong C-F bonds and fluorine-induced passivation, prevents decomposition at high voltages. However, PVDF-HFP is unsuitable as a standalone SPE due to its inherent mechanical weakness [48]. While hybridization methods such as solution casting and thermal curing exist, they fail to concurrently resolve mechanical fragility and interfacial instability and process efficiency-critical gaps filled by photopolymerization's rapid, precise, and versatile nature. Hybridizing PVDF-HFP with photocurable components via photocuring rapidly forms rigid, amorphous, crosslinked networks; these are the earliest reported photocured electrolytes [49]. This immobilizes PVDF-HFP, simultaneously boosting mechanical strength and resolving the stability/ionic mobility trade-off to create synergistic semi-interpenetrating networks. To further enhance mechanical strength, Çakmakçı et al. [50] reinforced a PVDF-HFP/PEGDA composite electrolyte using a polypropylene mesh and the resulting electrolyte to achieve room-temperature ionic conductivities of 5.4 mS/cm (for Li^+ conduction) and 3.3×10^{-3} mS/cm (for H^+ conduction), with a multi-fold increase in Young's modulus.

Kim et al. [51] optimized the TMPETA/PVDF-HFP ratio and HFP content to construct efficient ion-conduction channels, which enabled the photocured electrolyte to reach 85% of the liquid electrolyte's conductivity and significantly reduced interfacial resistance.

2.3. Gel Polymer Electrolytes with Ionic Liquids

Ionic liquids (ILs) have garnered significant attention in the electrolyte field due to their negligible volatility, high flash point, high thermal decomposition temperature, and

good ionic conductivity. However, the liquid nature of ILs also presents potential leakage risks and processing difficulties. To address these issues, researchers have explored combining ILs with other materials to fabricate polymer electrolytes with solid-state characteristics. From initial simple mixing to later chemical bonding, new methods for combining ILs with polymers have been continuously proposed. For instance, in 2013, Stepniak et al. [52,53] prepared a gel polymer electrolyte (GPE) via the photocrosslinking of ethoxylated bisphenol A diacrylate in the presence of the IL N-methyl-N-propylpiperidinium bis(trifluoromethanesulfonyl)imide. The IL-GPE exhibited a room-temperature ionic conductivity of 0.64 mS/cm. Porthault et al. [54] investigated the effect of radiation intensity of photocuring on the electrochemical properties of an IL-GPE using a similar crosslinker and IL. At a low radiation intensity of 0.7 mW/cm, the polymerization favored the formation of a low-crosslinking-density polymer with longer chains and a porous network, resulting in the highest ionic conductivity of 0.83 mS/cm at 25 °C. Conversely, at a high radiation intensity of 40 mW/cm, a dense crosslinked structure was formed, increasing the shear modulus to 182 kPa. This discovery established a structure–property relationship between polymerization kinetics and ion transport, providing a new approach for optimizing GPE performance through precise control of the photocrosslinking process.

Employing the fully fluorinated $TFSI^-$ anion, whose delocalized charge endows the IL-GPE with outstanding overall performance, is a common thread in these studies; however, the choice of cation varies. Due to the electrochemical stability conferred by conjugation, imidazolium ILs are more favored than their pyrrolidinium or piperidinium counterparts. By employing isobornyl acrylate as the monomer and trimethylolpropane triacrylate (TMPTA) as the crosslinker and IL 1-butyl-3-methylimidazolium bis(trifluoromethylsulfonyl)imide (BMITFSI), Lee et al. [55] fabricated an IL-GPE with a shear modulus over 100 MPa and room-temperature ionic conductivity of 0.3 mS/cm. Siddiquee et al. [56] developed an IL crystal elastomer electrolyte using an imidazolium IL with a long alkyl chain. By directly blending mono-/bi-functional mesogenic monomers (with one and two vinyl end-groups, respectively), IL 1-hexyl-3methylimidazolium bis(trifluormethyl sulfonyl)imide, plasticizer SN, and LiTFSI and photocuring, they fabricated an IL-GPE with continuous ion channels, thereby exhibiting 1.76 mS/cm room-temperature conductivity along with a high lithium-ion transference number of 0.61. The corresponding $Li/LiFePO_4$ battery demonstrated 98.8 mAh/g capacity retention over 160 cycles at 0.1C with 99% coulombic efficiency.

On the other hand, the research focus has also shifted towards further utilizing photopolymerizable ILs. In 2017, Lu et al. [57] proposed a novel Li^+-containing zwitterionic poly(ionic liquid) (PIL) electrolyte synthesized via the equimolecular neutralization of two solids, imidazolium-type zwitterion 3-(1-vinyl-3-imidazolio)propanesulfonate (VIPS) and LiTFSI. Using photocuring, they fabricated free-standing PIL electrolyte films with good mechanical strength. Adding an appropriate amount of propylene carbonate (PC) to promote lithium ion dissociation enhanced the room-temperature ionic conductivity to the level of ~0.1 mS/cm, with a lithium-ion transference number of 0.20. The team proposed a potential "Li^+-rich channels" mechanism within the system, paving the way for subsequent research. López et al. [58] used microporous aramid scaffolds by infiltrating the photopolymerizable IL (1-(2-methacryloyloxy)ethyl-3-butylimidazolium bis(trifluoromethanesulfonyl)imide, ILQ), along with anther IL and LiTFSI, into the interconnected microchannels of microporous aramids. Following the photopolymerization of ILQ with crosslinker ethyleneglycol dimethacrylate, this approach established a synergistic dual-stabilization mechanism combining physical confinement by the aramid framework and the chemical cross-linking of the PIL network. The resulting electrolyte achieved a high ionic conductivity of 1.23 mS/cm at 25 °C with only 45% of the liquid components retained.

In summary, while increasing the plasticizer content is the most straightforward and effective way to boost ionic conductivity, replacing it with ILs can avoid the accompanying compromise in high-voltage performance. Introducing long alkyl chains to IL induces liquid–crystalline phases in IL-GPEs, thereby creating ordered pathways for ion transport that help raise the lithium-ion transference number. It is also worth noting that using photopolymerizable ILs to directly form the electrolyte matrix represents an important direction for future development.

2.4. Single-Ion-Conducting Polymer Electrolytes

Single-ion-conducting polymer electrolytes (SICPEs) feature immobilized anions covalently bonded to the polymeric matrix as shown in Figure 3, enabling high lithium-ion transference numbers that minimize electrode polarization and suppress dendrite growth. Commercially available vinyl-containing lithium salts make it convenient to synthesize SICPEs through photopolymerization.

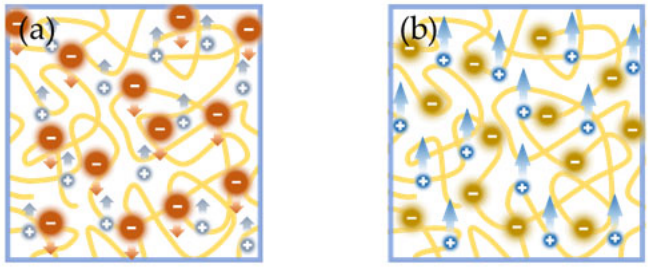

Figure 3. Schematic illustration of (**a**) dual-ion-conducting and (**b**) single-ion-conducting polymer electrolytes.

Building upon the previously described strategy of Lu's, Yu et al. [59] further optimized the IL-GPE formula via the equimolar mixing of VIPS and the lithium salt 4-styrenesulfonyl(trifluoromethylsulfonyl)imide (LiSTFSI). The photocrosslinker effectively anchored most anions covalently within the polymeric matrix, achieving a lithium-ion transference number of 0.94 while increasing the ionic conductivity at 30 °C to 0.13 mS/cm. This molecular design successfully achieved the synergistic optimization of the high transference number and enhanced ionic conductivity in single-ion conductors.

Jiang et al. [60] employed photocrosslinking to develop a PEO-based semi-interpenetrating polymer electrolyte, which enhanced mechanical strength while maintaining ionic conductivity. Following this approach, Guan et al. [61] developed an interpenetrating network SICPE that demonstrated superior synergy by integrating dual networks: a gel network as well as another network containing photocrosslinked LiSTFSI. This interpenetrating network enhanced mechanical robustness (0.50 MPa compressive strength vs. 0.39 MPa in single networks), enabling higher room-temperature conductivity of 0.19 mS/cm.

Another distinct architecture that adopted a photopolymerization technique to fabricate SICPEs, addressing the enhancement in lithium-ion transference number, was demonstrated by Sutton et al. [62]. They proposed a single-network design, incorporating oligomer poly[lithium 1-(3-methacryloyloxy)propylsulfonyl]-1-(trifluoromethylsulfonyl)imide (PLiMTFSI) as the dangling chain in a linear molecule, which enables efficient Li^+ transport along the polymer backbone, exhibiting higher segmental mobility and mitigating potential interfacial contact issues associated with high crosslinking density. While achieving a transference number of 0.85, excessively long PLiMTFSI chains may result in elevated local viscosity and impede Li^+ dissociation, hindering their migration into the PEG conduction phase.

2.5. Organic–Inorganic Hybrid Electrolytes

In the development of high-performance solid electrolytes, it has been found that pure polymer electrolytes often face bottlenecks such as low ionic conductivity, insufficient mechanical strength, and low thermal stability. To overcome these limitations, the incorporation of inorganic contents into polymeric matrices to obtain hybrid electrolytes is an effective modification strategy.

The initiator-free thiol-ene photopolymerization method is widely adopted in industrial production due to its high tolerance to oxygen and moisture, avoiding the detrimental impact of initiator residues on electrochemical performance. Zuo et al. [63] first reported this strategy for fabricating photocured SPEs without photoinitiators through thiol-ene photopolymerization. The utilized polyhedral oligomeric silsesquioxane (POSS-SH) generates thiyl radicals directly under UV irradiation, and the radicals subsequently undergo additional reactions with PEGDMA, forming a hybrid organic–inorganic network. This design enhances mechanical properties via the rigid POSS core while leveraging the PEG segments to provide ion transport channels, achieving a tensile strength of 1.7 MPa and a room-temperature ionic conductivity of 0.21 mS/cm. To balance high mechanical strength and ionic conductivity, the same team further introduced a poly(ε-caprolactone)-b-poly(ethylene glycol)-b-poly(ε-caprolactone) triblock copolymer (PCL-b-PEG-b-PCL, HTPE) end-functionalized with methacrylate groups as the crosslinker, which was also covalently integrated with the POSS core via initiator-free thiol-ene photopolymerization [64]. They found that, as the PCL segment length increases, the tensile strength of HTPEs peaked for HTPE20, while the ionic conductivity reaches its maximum for HTPE30. The integration of flexible organic segments with the inorganic POSS core suppressed the crystallinity of polyester domains. This not only increased the tensile strength to 9.57 MPa but also significantly enhanced the lithium-ion transference number to 0.61 and the ionic conductivity to 3.36 mS/cm (at 100 °C), owing to the lithium salt dissociation promoted by the ester carbonyl groups in PCL. The system demonstrated stable cycling performance in $LiFePO_4$ full cells, validating its high-voltage compatibility.

In addition to photocuring organosilicon nanoclusters, incorporating inorganic nanomaterials as fillers into resins is a primary method for preparing organic–inorganic hybrid electrolytes. Hu et al. [65] developed a cross-linked organic–inorganic hybrid network via the above-mentioned thiol-ene photopolymerization of thiol-modified SiO_2 nanoparticles and PEGDA, achieving an ionic conductivity of 0.73 mS/cm at 30 °C. Simultaneously, the lithium-ion transference number was enhanced to 0.74 due to the scavenger effect of silica nanoparticles. Lyu et al. [66] utilized the KH570 silane coupling agent to modify SiO_2. During the photocuring process, the modified SiO_2 reacted with PEGDA, enabling the inorganic filler to act as active nodes in the cross-linking network and significantly reducing the crystallinity of PEO. The resulting cross-linked network lowered the glass transition temperature of the composite electrolyte to below −50 °C. Simultaneously, the Lewis acid centers of the modified SiO_2 promoted the dissociation of LiTFSI, allowing the electrolyte to maintain an ionic conductivity of 0.17 mS/cm at 0 °C. This approach substantially improved the low-temperature performance of solid-state batteries.

Choi et al. [67] fabricated an asymmetric coating of a garnet-type $Li_7La_3Zr_2O_{12}$ (LLZO) particle-polymer slurry on one side of a cellulose membrane. The LLZO was immobilized via photocuring exclusively on the electrolyte side facing the lithium metal. In addition to forming a physical barrier against lithium dendrites, the LLZO particles suppressed the local current concentration by promoting the uniform distribution of Li^+ flux at the interface. Simultaneously, anion immobilization on the LLZO surface led to an increased lithium-ion transference number. Karuppiah et al. [68] further achieved the 3D printing of Ta-doped LLZO via DLP. After the debinding and sintering processes, they eliminated interlayer

defects to obtain a dense inorganic solid electrolyte, which achieved a room-temperature ionic conductivity of 0.003 mS/cm.

Wang et al. [69] introduced montmorillonite (MMT) nanosheets into the photocured interpenetrating network formed by PEGMEA and PEGDA. By leveraging the layered structure and local electric field effects within the interlayers, MMT promotes LiTFSI dissociation and provides Li^+ transport highways. This design elevates the ionic conductivity to 1.06 mS/cm and achieves a lithium-ion transference number of 0.79. Bae et al. [70] expanded the interlayer spacing of illite (EI), another layered clay mineral, using an acid treatment–microwave expansion process, and uniformly immobilized it within an TMPETA crosslinked network via photocuring. The expanded layered structure of EI provided additional ion channels, enabling the polymer electrolyte to achieve an ionic conductivity of 10.8 mS/cm at 20 °C.

The demand for flexible devices has driven the application of one-dimensional fillers. Zhu et al. [71] fabricated a composite electrolyte via the photopolymerization of butyl acrylate copolymerized with PEGDA containing halloysite nanotubes (HNTs). By leveraging the dual-wall charge characteristics of HNTs, where the inner Al_2O_3 layer adsorbs $TFSI^-$ through positive charges and the outer SiO_2 layer attracts Li^+ through negative charges, they enhanced lithium-ion mobility and established directional ion-conducting channels. Furthermore, this process endowed the electrolyte with over 420% elongation at break and 3 MPa tensile strength.

Beyond physically blending inorganic nanomaterials with resin, the aggregation of nanomaterials can also be avoided by mixing their precursors with the resin. Wu et al. [72] developed a photocured polyurethane acrylate-based nanocomposite polymer electrolyte via the in situ hydrolysis of tetrabutyl titanate to generate uniformly dispersed TiO_2 nanoparticles, combined with an IL; the electrolyte exhibited an ionic conductivity of 1.05 mS/cm and mechanical strength of 1.01 MPa. Wang et al. [73] proposed a similar strategy that co-constructs the ionogel through processes including the condensation of tetrabutyl titanate via a non-hydrolytic sol–gel process to form TiO_2 and the polymerization of BA, which displayed an ionic conductivity of 1.34 mS/cm at 30 °C. The TiO_2 network provided the ionogel with a tensile strength of 0.32 MPa, while the long BA chains provide hyperelasticity with a fracture strain of 856%. These components synergistically resolve the intrinsic "strength–ductility" conflict in conventional ionogels. A customized stretchable battery setup using this ionogel achieves stable power output under 50% tensile strain.

Collectively, different types of inorganic contents play diverse roles through their unique physicochemical properties. The organosilicon can form stable interfaces with the electrodes. The ceramic particles enhance mechanical properties and thermal stability while improving chain segment mobility by reducing polymer crystallinity. The tubular materials provide anisotropic ion transport channels. The layered silicates facilitate lithium salt dissociation through their interlayer charge separation effect. Eventually, rapid in situ photocuring not only prevents filler sedimentation in slurries during processing but also establishes robust organic–inorganic interfaces at the molecular level, thereby maximizing the effectiveness of the inorganic contents.

2.6. 3D Electrolytes

VPP demonstrates unique advantages in the 3D printing of electrolytes, which introduces a new degree of structural freedom into electrolyte fabrication beyond just material composition [74]. With its high precision and complex structural forming capabilities, VPP offers novel solutions to the interfacial contact and ion transport challenges in conventional solid-state batteries. In 2017, Chen et al. [75] used projection micro-stereolithography (μSLA) to fabricate zigzag-shaped PEGDA-based GPEs. Their designed 2.5D and 3D lattice

structures not only achieved shape adaptability of the electrolyte but also significantly improved interfacial ion transport efficiency by increasing the electrode–electrolyte contact area, achieving an ionic conductivity of 4.8 mS/cm.

Yu et al. [76] proposed a "photoinitiation inhibitor" mechanism, utilizing a rose bengal/N-phenylglycine system to regulate photopolymerization kinetics. By inducing phase separation through laser interference patterns, they constructed a holographic polymer electrolyte with a 740 nm periodic structure, which serves as a highly ordered ion-conducting network. This approach enhanced ionic conductivity by five orders of magnitude, demonstrating the synergistic optimization of optical and electrochemical properties.

He et al. [77] employed the SLA technique to print an Archimedean spiral-structured PEGDA/LiTFSI solid electrolyte, which increased the interfacial contact area by 95%, enhanced interfacial adhesion and achieved a room-temperature ionic conductivity of 0.37 mS/cm, which is an order of magnitude higher than conventional planar electrolytes. This 3D architecture shortened Li^+ transport pathways, enabling LFP full cells with a high loading of 5 mg/cm^2 to maintain excellent cycling performance, retaining 77% capacity after 250 cycles, far surpassing the 19% retention of planar electrolytes. This work confirmed the critical role of 3D structural design in reducing interfacial impedance.

Maurel et al. [78] systematically investigated the influence of PEGDA molecular weight on the performance of DLP-printed electrolytes, providing crucial guidance for material selection. They found that a 575 + 700 g/mol blend system achieved an optimal balance between printing precision and electrochemical performance, maintaining 6.26 MPa mechanical strength while delivering an ionic conductivity of 1.2 mS/cm at 80 °C. By optimizing exposure time and light intensity, they successfully printed 2.5D and 3D lattice structures with <5% dimensional error, showcasing the unique advantages of 3D printing in fabricating complex-shaped electrolytes.

Martinez et al. [79] fabricated GPEs for sodium-ion batteries via photopolymerization, demonstrating superior oxidative stability (up to 4.8 V vs. Na^0/Na^+) compared to liquid electrolytes (which began decomposing at 3.5 V). Their work combined DLP-printed GPEs with direct ink writing (DIW)-printed $Na_{0.44}MnO_2$ electrodes, showcasing the potential of multiprocess additive manufacturing for complete battery fabrication.

Although other monomers such as acrylamide [80] and urethane acrylate [81] were also studied in electrolyte VPP 3D printing to leverage their Li^+ coordination ability and thereby enhance ion dissociation and mobility, PEGDA still remains the most studied primary material for 3D-printed electrolytes. However, PEGDA is not specifically tailored for battery applications, leaving significant untapped potential. As demonstrated in previous studies, various photocurable materials have been derived. They can further enhance electrolyte performance when combined with 3D printing, providing higher ionic conductivity, improved mechanical strength, and superior stability.

Other than printing actual electrolytes via VPP, the technology can also be employed to create sacrificial 3D templates. These templates enable the molding of non-photocurable materials into customized architectures through subsequent processes such as calcination [82], thereby granting unconventional geometries to materials incompatible with VPP techniques.

2.7. In Situ Photocured SPEs

In situ polymerized electrolytes provide remarkable advantages [83]. The in situ polymerization process enables perfect wetting at the electrode–electrolyte interface, where monomer precursors penetrate electrode pores and form a continuous network, effectively solving the poor interfacial contact issues inherent in traditional external electrolyte membranes (Figure 4). The in situ formed polymeric interphase simultaneously constructs stable

protective layers. The process is compatible with various polymerization methods including photopolymerization and photocrosslinking and can be integrated with 3D printing for precise electrolyte patterning.

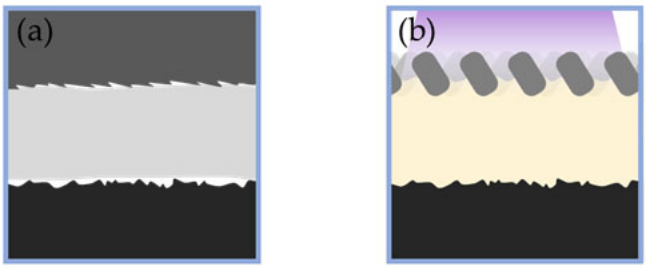

Figure 4. The schematic illustration of the cross-section of (**a**) a conventional SPE between electrodes and (**b**) an in situ photocured SPE with an adaptively optimized, light-permeable electrode.

Yuan et al. [84] proposed a novel method for the in situ construction of an integrated cathode–solid electrolyte structure via photocuring. First, a mixed polymeric solution was coated on the $LiFePO_4$ (LFP) cathode, and a porous framework was formed after dissolving the polyvinyl pyrrolidone. Then, a monomer solution was infiltrated and photo-cured to achieve intimate interfacial contact between the electrolyte and cathode. The battery exhibited a reversible capacity of 153 mAh/g at 25 °C and retained ~145 mAh/g after 150 cycles, significantly outperforming conventional solid-state batteries. Lin et al. [85] constructed a polypyrrole-citral nitrile copolymer coating layer in situ on the surface of $LiNi_{0.8}Co_{0.1}Mn_{0.1}O_2$ via photocuring. The cross-linked network structure prevents swelling due to electrolyte absorption, while the delocalized π-bonds of polypyrrole enhance electron conduction, and the cyano groups coordinate with the transition metal ions of the cathode to ensure the continuity of the coating. This electrolyte maintains structural stability under extreme conditions (60 °C high temperature, 4.5 V high voltage, and 3C high rate), providing a novel strategy for high-energy-density batteries in harsh environments. To address the bottleneck of physical electrode–electrolyte contact in lithium–oxygen batteries, Cui et al. [86] directly photocured a PVDF-HFP-based GPE onto the RuO_2@C air cathode via in situ photopolymerization, achieving integrated fabrication, which reduced interfacial impedance by 65% and increased cycle life by 8.5 times.

The conformal polymer coating uniformly covering the 3D foam structure is a key advantage of in-situ photopolymerization. While sulfur-loaded foam materials effectively enhance the areal capacity of sulfur cathodes, their highly porous structure increases the electrolyte contact area, exacerbating polysulfide dissolution [87]. To address this, Ahn et al. [88] fabricated a polymer layer in situ via photopolymerization on Al foam sulfur cathodes, incorporating monomer 2-acrylamido-2methylpropane sulfonic acid and PEGDA crosslinkers. The sulfonate groups selectively conduct Li^+ while electrostatically repelling polysulfides. This polymer layer enabled the Li-S pouch cells with 1 mg/cm^2 sulfur loading to achieve a discharge capacity of 535 mAh/g (96% Coulombic efficiency) after 40 cycles, significantly outperforming uncoated cathodes (389 mAh/g, 22% efficiency).

Xie et al. [89] utilized a 3D textile-structured light-permeable composite lithium anode that enables light penetration through its porous structure to cure the electrolyte, achieving the synchronous one-step in situ photopolymerization bonding of both cathode and anode to form seamless dual-interface connections. This design enables symmetric cells to cycle stably for 1000 h at 0.5 mA/cm^2, with LFP full cells maintaining 84% capacity retention after 500 cycles and a 56% reduction in interfacial resistance compared to conventional stacked cells. It demonstrates compatibility with high-loading cathodes and 4.3 V high-voltage cathodes. Benefiting from the integrated interface design, a flexible pouch cell maintains a

stable 3.38 V plateau after over 1000 bending cycles at a 10 mm bending radius, offering a new solution for wearable applications.

To summarize, photocured electrolytes, as the most technologically mature photocurable component in batteries, have developed distinct paradigms. For photocurable monomers, acrylate derivatives featuring flexible segments (e.g., PEGMA) and tailored functional groups (e.g., piperidinium-containing ionic liquids or lithium-dissociable organic salts) that enable the homogeneous integration of novel properties to the polymeric matrix will become prominent. Additives beyond photocurable components remain an indispensable part of current photocured electrolytes. Plasticizers with asymmetric molecular structures and appropriate chain lengths (e.g., GN) help enhance ionic conductivity, while initiator-free systems achieved through reactions like thiol-ene chemistry, combined with the incorporation of organosilicon (e.g., POSS-SH) to form uniform organic-inorganic hybrids, contribute to improved electrolyte stability.

However, a comparison between mature commercial electrolytes and emerging photocured electrolytes reveals a significant gap in the latter's performance. The widely used 1 M $LiPF_6$ in binary carbonate solvent system liquid electrolytes demonstrates high ionic conductivity (~10 mS/cm at 25 °C [90]). In contrast, photocurable solid polymer electrolytes typically exhibit conductivity an order of magnitude lower due to restricted ion movement in the polymeric matrix, though this can be enhanced through plasticizer additives. Additionally, the photocuring process has a higher transference number. Mechanically, commercial polyolefin separators maintain superior tensile strength of 100–200 MPa and a Young's modulus of 0.5–1.5 GPa, and these advantages are retained even after the separator is swelled by liquid electrolytes [91]. This is attributed to their ultra-high molecular weight and high crystallinity, while photocurable electrolytes generally show weaker mechanical properties. In both of these aspects, photocurable electrolytes still fall short of commercial standards. However, photocuring still possesses substantial development potential due to its inherent advantages, such as compatibility with 3D printing, in situ processing, and single lithium-ion-conducting SPE fabrication.

3. Membranes

Polymerization-induced phase separation (PIPS) is a technique that utilizes polymerization to prepare biphasic materials [92,93]. In this process, an initially homogeneous mixture of monomer and solvent undergoes phase separation during photoinitiated polymerization, resulting in the formation of a bicontinuous structure comprising a polymer phase and a solvent phase (Figure 5). The former provides mechanical integrity, while the latter serves as a porogen and forms ion transport channels. Non-contact in situ PIPS can be achieved via photopolymerization, a technique that has been utilized for the fabrication of photocured separators. Since PIPS enables the direct preparation of porous materials, this technology may find new applications in 3D printing [94,95].

Ihrner et al. [96] employed a hybrid precursor combining bisphenol A dimethacrylate with and without ethoxylate segments, blended with carbonate-based solvents; they then synthesized a bicontinuous phase structure through PIPS. By adjusting the monomer composition, the phase-separated domain size was controlled from the nanometer scale to the micron scale. They found that enhancing the proportion of the monomer with flexible ethoxylate segments improved polymer–solvent compatibility while maintaining mechanical strength, resulting in a more homogeneous bicontinuous phase structure. While using only bisphenol A ethoxylate dimethacrylate, Emilsson et al. [97] introduced the thiol monomer TEMPIC to improve network homogeneity and brittleness issues through a thiol-ene reaction, enabling a reduction in film thickness while increasing the Young's modulus to 880 MPa.

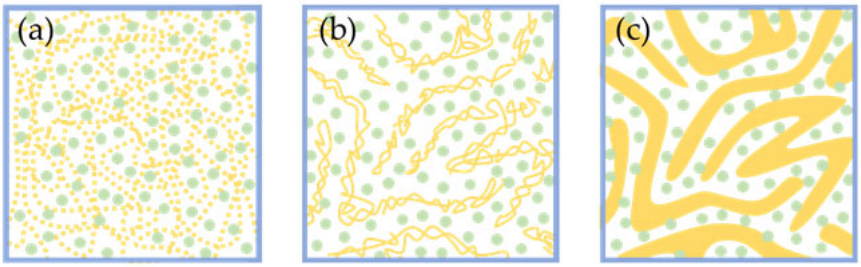

Figure 5. Schematic illustration of the process associated with photopolymerization-induced phase separation: (**a**) the dissolved photoactive components are evenly distributed in the solvent. (**b**) The photoactive components start to polymerize under irradiation. (**c**) A bicontinuous structure of the polymer and the original solvent is formed.

Manly et al. [98] developed a photocuring system based on the 1,4-butanediol diacrylate monomer and ethylene carbonate solvent. By controlling the phase separation process, they successfully fabricated a separator with 38.5% porosity and 1.98 mS/cm conductivity. The 22 nm pore structure is beneficial for suppressing lithium dendritic penetration. Furthermore, it shows no thermal shrinkage and no fusion behavior at 150 °C, outperforming commercial separators. They addressed the insufficient mechanical strength of previous systems by introducing PEGDA as the comonomer into the original formulation. Through controlling the photocuring kinetics to improve the monomer conversion rate, the separator's elastic modulus was significantly enhanced from 272 MPa to 450 MPa [99].

4. Anodes

Currently, the vast majority of reported studies on 3D electrodes fabricated using VPP do not directly print electrochemically active materials via photocuring. Instead, they either print resins containing precursors of the electrochemically active materials followed by post-processing to obtain 3D electrodes (Figure 6) or create scaffold structures via VPP and subsequently deposit electrochemically active materials using other methods [100].

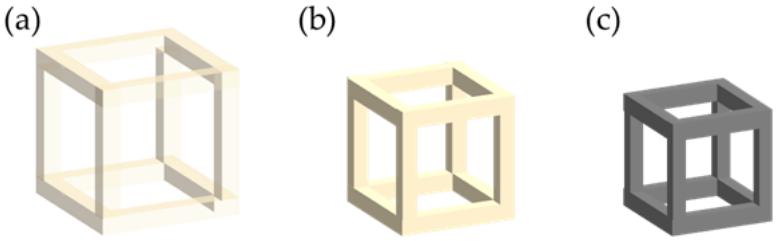

Figure 6. Schematic illustration of the process of fabricating electrodes via photocuring. (**a**) VPP of the precursors of active materials mixed with resins to obtain the "green part". (**b**) Debinding of the polymerized resin to obtain the "brown part". (**c**) Sintering at high temperatures to achieve densification.

Due to the high packaging volume ratio in conventional 2D microbatteries limiting energy density miniaturization, Wang et al. [101] first utilized an SU-8 negative photoresist through mask-projection UV photolithography combined with a two-step pyrolysis process to fabricate high-aspect-ratio carbon post arrays with minimum diameters of 20 μm. This significantly increased the electrode surface area. They demonstrated that the photolithographically patterned 3D structures provided 80% higher areal capacity compared to unpatterned carbon films with identical projected areas. However, this process exhibited limited architectural freedom. Narita et al. [102] employed DLP to replace mask-projection photolithography and fabricated structures with various complex 3D architectures spanning micrometers to centimeters. Following stepwise pyrolysis, the resulting glassy carbon electrodes with periodic lattice structures featured straight through-pores that optimized

ion transport pathways. These achieved a high areal capacity of 3.2 mAh/cm at 2.4 mA/cm. Combining O_2 plasma etching to reduce feature sizes and roughen surfaces decreased electrode-diffusion time, enabling a 2.5-fold improvement in rate capability at 300 mA/g.

Wang et al. [103] addressed challenges of particle agglomeration during pyrolysis and disordered carbon matrix regulation in silicon oxycarbide (SiOC) materials. They employed dental methacrylates as the photoactive carbon source and a silane coupling agent methacryloxypropyltrimethoxysilane (MPTMS) as the silicon precursor. Through visible-light-triggered rapid photopolymerization, molecular-level homogeneous mixing was achieved, suppressing phase separation during high-temperature pyrolysis. This successfully embedded 2 nm SiOC particles within the carbon matrix. The photopolymerization formed a highly cross-linked network in the SiOC precursor, enabling optimization of the disordered/ordered carbon ratio by tuning the mass ratio of the coupling agent. At a mass ratio of 0.50, the disordered carbon content reached its maximum, and the electrode maintained a capacity of 443 mAh/g after 50 cycles at 100 mA/g, representing a 40% improvement over the bare carbon electrode. The superior capacity retention rate resulted from a synergistic buffering mechanism whereby the rigid SiOC nanoparticles anchor the carbon matrix to resist damage during cycling, while the carbon matrix provides electrical conduction, shields SiOC from the electrolyte, and cushions its volume changes. These effects are evidenced by the high coulombic efficiency after 50 cycles and the absence of ongoing electrolyte decomposition revealed by cyclic voltammograms, confirming SiOC–electrolyte compatibility and the formation of a stable SEI layer. Ali et al. [104] further applied photocuring to address volume expansion issues in silicon-based materials. By combining freeze-drying with photopolymerization, they constructed a three-dimensional interconnected porous framework. This ensured subsequent uniform SiO_2 deposition within the pore channels via chemical vapor deposition. Their resulting SiO_2-C material possesses a silicon content of 59.8 wt%, leveraging carbon matrix buffering for volume changes; it delivered an initial discharge capacity of 719 mAh/g and retained 693 mAh/g after 100 cycles.

Ding et al. [105] first proposed the organic molecule confinement reaction (OMCR) strategy, which utilizes spontaneous emulsification of a photoactive oil phase with an aqueous phase to form a uniform nanodroplet reactor. After adding tin precursor $SnCl_4$, through photopolymerization of the emulsion, a 3D organic nanoframe was constructed. A subsequent hydrothermal reaction and confinement reduction led to the formation of a Sn nanoparticle composite anode with nanovoids embedded within a two-dimensional laminar matrix of graphene nanosheets. This effectively suppressed the volume expansion issue of the Sn anode, enabling the battery to achieve a high cycling capacity of 539 mAh/g after 200 cycles with a Sn loading of 19.58 wt%. Addressing the demands for high solid loading and structural optimization, Wang et al. [106] developed a photocurable system based on a difunctional methacrylate resin. This system integrates TiO_2, a Sn-based precursor dibutyltin dilaurate, and a SiO_x porogen agent into the cross-linking network. Following photopolymerization, carbonization, and HF etching, a mesoporous $TiO_2/SnO_2/Sn/C$ nanohybrid was formed, which enabled the battery to maintain a high reversible specific capacity of 452 mAh/g after 400 cycles. Building on this foundation for potential applications utilizing TiO_2-rich resources such as lunar regolith, Maurel et al. [107] employed a photocurable resin loaded with 18 wt% TiO_2 particles. Utilizing DLP 3D printing equipped with a conveyor belt system, they achieved the precise fabrication of complex sodium battery anodes. The interconnected pore channels within the specifically designed gyroid structure enhanced ionic diffusion efficiency and active material utilization. Consequently, the TiO_2 anode delivered a capacity of 63 mAh/g at 1 mA/g.

5. Cathodes

Martinez et al. [108] employed a powder-based resin strategy by directly dispersing $LiCoO_2$ particles and conductive carbon black into a photosensitive resin, achieving electrode printing with microporosity via DLP photopolymerization. Half-cell tests demonstrated that sintered electrodes delivered capacities of 160 mAh/g (approaching commercial performance), whereas unsintered "green state" electrodes exhibited significantly reduced capacities due to the presence of insulating resin. However, particle sedimentation-induced compositional segregation and light scattering issues still limit the printing accuracy for complex geometries. Yee et al. [109] first reported a strategy for photopolymerizing metallic salt precursors based on hydrogels, which involved mixing an aqueous solution of $LiNO_3$ and $Co(NO_3)_2$ (precursors for $LiCoO_2$) with PEGDA, subsequently achieving 3D printing with ~100 μm resolution using DLP. This method eliminated light scattering by solid particles in traditional slurries, making photopolymerization easier to implement and enabling higher resolution. Synthesis of binder-free $LiCoO_2$ electrodes was realized through high-temperature calcination, with their half-cells demonstrating 76% capacity retention after 100 cycles at C/10. While establishing the technical foundation for the photocurable precursor approach, the calcination process incurred large mass losses and volumetric shrinkage, leading to fragile structures. The electrodes also showed poor rate capability, prompting the authors to suggest performance improvements through refined electrode geometry.

Martinez et al. [110] extended the precursor approach to the ternary material $LiNi_{1/3}Mn_{1/3}Co_{1/3}O_2$ (NMC 111), using nitrates as precursors, and successfully printed complex lattice structures. It should be noted that sintering conditions play an important role in the battery performance as the electrodes prepared at 600 °C exhibited incomplete crystallization, resulting in increased side reactions, while sintering at 900 °C caused severe lithium volatilization and low cation mixing between Li^+ and Ni^{2+}, impeding Li^+ deintercalation kinetics and exacerbating polarization. Although a sintering temperature of 700–800 °C could balance electrochemical performance and cation ordering, mechanical integrity remained a bottleneck, as the slow heating rate reduced cracking but resulted in lattice defects due to extended thermal exposure time. These factors collectively contributed to capacity loss.

In the exploration of stereolithography for lithium–sulfur battery cathodes, Saccone et al. [111] developed emulsion stereolithography. By stabilizing a water-in-oil emulsion resin containing an aqueous Li_2SO_4 precursor solution with surfactants, they successfully printed Li_2S-C composite cathodes with 50 μm features, marking the first report of the additive manufacturing of Li_2S composites. After pyrolysis, the electrodes demonstrated 86.6% capacity retention after 50 cycles in Li-S batteries. The innovation lies in resolving the compatibility issue between the water-soluble precursor and the organic photopolymer resin via emulsification, circumventing the challenge of directly processing air-sensitive materials.

6. Other Battery Components

The current collector and casing contribute heavily to the overall weight of batteries, yet this portion currently represents "dead weight" in terms of energy storage functionality. By integrating them with other battery components, batteries may achieve more efficient space utilization and weight reduction, thereby fully utilizing the "dead weight".

Gulzar et al. [112] fabricated battery casings with body-centered cubic porous structures using SLA, employing sputtered metal coatings to enhance conductivity and corrosion resistance. The battery, fabricated by infilling electrode slurries into the porous structures, demonstrated a stable capacity of 1.86 mAh, outperforming conventional metallic coin cells.

Cohen et al. [113] employed SLA and other 3D-printing techniques to fabricate polymer substrates with interconnected channels, which were then metallized via electroless plating to form current-collector layers, followed by sequential electrophoretic deposition of the cathode, electrolyte, and anode. The microbatteries assembled using the substrates demonstrated areal capacities of 400–500 $\mu Ah/cm^2$ at 0.1C and achieved energy densities three times higher than those of conventional planar thin-film batteries.

Martinez et al. [114] fabricated a 3D porous copper current collector with a compressive strength of 19 MPa and an electrical conductivity of 3.09×10^3 S/m by employing DLP to print a 3D resin structure, infiltrating it with copper nitrate, followed by sintering and reduction. This lithium-ion structural battery integrates both load-bearing and energy storage functions. After the electrophoretic deposition of the graphite anode material, half-cell testing demonstrated a first-cycle discharge capacity of 371 mAh/g, approaching the theoretical capacity of graphite.

7. Conclusions

Photocuring and photocuring-based additive manufacturing, i.e., vat photopolymerization, have demonstrated transformative potential in advancing next-generation battery technologies, bridging the gap between complex design and functional performance. By enabling high-resolution, geometrically complex, and customizable battery components, photocuring overcomes the key limitations of conventional manufacturing, such as poor interfacial contact, limited design flexibility, and trade-offs between electrochemical and mechanical properties. This review systematically summarizes recent progress in photocured electrolytes, membranes, anodes, and cathodes, highlighting how material innovation and 3D structural engineering synergistically enhance ionic conductivity, mechanical robustness, and electrochemical stability.

Despite these advancements, critical challenges remain before industrial adoption can be realized, particularly concerning technology maturity, scalability, and throughput:

(1) Most commercially available photocurable resins lack intrinsic electrochemical activity, necessitating post-processing to convert them into functional battery materials, which adds complexity and may compromise structural integrity. Limitations in materials currently restrict demonstrations primarily to the laboratory scale.
(2) Multi-material integration remains challenging due to the incompatibility of post-processing protocols, solvents' non-orthogonality, and disparities in curing rates. Current studies focus solely on photocuring single battery components such as the electrolyte or electrodes, while batteries incorporating multiple photocured components, let alone fully photocured batteries, remain entirely unexplored.
(3) While VPP excels in prototyping, its processing speed and applicability to large-scale production are significantly constrained, which is primarily due to the relatively small area that can be simultaneously processed by light. Laser-based techniques such as SLA and TPL are particularly limited by throughput and thus may be more suitable for the microbattery industry.

The convergence of photocuring and 3D printing is poised to unlock new paradigms in battery architecture and redefine battery manufacturing, enabling customized energy storage solutions for different applications. However, bridging the gap between lab-scale innovation and industrial adoption will require concerted efforts to address the above challenges, with a focus on developing energy-storage-specific resins, integrated structural/compositional designs, and advanced high-throughput VPP techniques. By embracing emerging technologies to overcome existing material- and processing-related challenges, photocuring could ultimately pave the way for batteries featuring the monolithic integration of components. Such seamless structures, along with the greater structural

freedom afforded by 3D printing, have the potential to unlock higher performance in future batteries.

Author Contributions: Conceptualization, Z.L., Y.L. and M.C.; writing—original draft preparation, Z.L.; writing—review and editing, Y.L., M.C. and W.L.; supervision, W.L. and X.W.; project administration, X.W. All authors have read and agreed to the published version of the manuscript.

Funding: This work was partially supported by the National Natural Science Foundation of China (NSFC) (62435005, 62375087 and 12374304), the National Key R&D Program of China (2024YFB3613500), the Key-Area Research and Development Program of Guangdong Province (2023B0909010002), the Introduced Innovative Team Project of Guangdong Pearl River Talents Program (2021ZT09Z109), the Xiaomi Young Talents Program (Xiaomi Foundation), and the Chinese Postdoctoral Science Foundation—CETC Joint Support Program (2025M773369).

Conflicts of Interest: The authors declare no conflicts of interest.

References

1. Li, Z.; Wei, X.; Yang, Z. Pulsed Laser 3D-Micro/Nanostructuring of Materials for Electrochemical Energy Storage and Conversion. *Prog. Mater. Sci.* **2023**, *133*, 101052. [CrossRef]
2. Long, J.W.; Dunn, B.; Rolison, D.R.; White, H.S. 3D Architectures for Batteries and Electrodes. *Adv. Energy Mater.* **2020**, *10*, 2002457. [CrossRef]
3. Shaju, A.; Ummer, R.P.; Thomas, S.; Kandasubramanian, B. Novel Approaches in 3D Printing Techniques for the Development of High-Performance Micro-Batteries. *J. Electron. Mater.* **2025**, *54*, 1531–1552. [CrossRef]
4. Narita, K.; Saccone, M.A.; Sun, Y.; Greer, J.R. Additive Manufacturing of 3D Batteries: A Perspective. *J. Mater. Res.* **2022**, *37*, 1535–1546. [CrossRef]
5. Mottaghi, M.; Pearce, J.M. A Review of 3D Printing Batteries. *Batteries* **2024**, *10*, 110. [CrossRef]
6. Yang, Y.; Yuan, W.; Zhang, X.; Yuan, Y.; Wang, C.; Ye, Y.; Huang, Y.; Qiu, Z.; Tang, Y. Overview on the Applications of Three-Dimensional Printing for Rechargeable Lithium-Ion Batteries. *Appl. Energy* **2020**, *257*, 114002. [CrossRef]
7. Mu, Y.; Chu, Y.; Pan, L.; Wu, B.; Zou, L.; He, J.; Han, M.; Zhao, T.; Zeng, L. 3D Printing Critical Materials for Rechargeable Batteries: From Materials, Design and Optimization Strategies to Applications. *Int. J. Extrem. Manuf.* **2023**, *5*, 042008. [CrossRef]
8. Huo, S.; Sheng, L.; Su, B.; Xue, W.; Wang, L.; Xu, H.; He, X. 3D Printing Manufacturing of Lithium Batteries: Prospects and Challenges toward Practical Applications. *Adv. Mater.* **2024**, *36*, 2310396. [CrossRef] [PubMed]
9. Zhang, F.; Zhu, L.; Li, Z.; Wang, S.; Shi, J.; Tang, W.; Li, N.; Yang, J. The Recent Development of Vat Photopolymerization: A Review. *Addit. Manuf.* **2021**, *48*, 102423. [CrossRef]
10. Shah, M.; Ullah, A.; Azher, K.; Rehman, A.U.; Juan, W.; Aktürk, N.; Tüfekci, C.S.; Salamci, M.U. Vat Photopolymerization-Based 3D Printing of Polymer Nanocomposites: Current Trends and Applications. *RSC Adv.* **2023**, *13*, 1456–1496. [CrossRef] [PubMed]
11. Yang, W.; Zhang, M.; Peng, S.; Pan, R.; Liu, Y. Introduction to Vat Polymerization 3D Printing Technologies. In *Vat Photopolymerization Additive Manufacturing*; Elsevier: Amsterdam, The Netherlands, 2024; pp. 1–28, ISBN 978-0-443-15487-4.
12. Huang, J.; Qin, Q.; Wang, J. A Review of Stereolithography: Processes and Systems. *Processes* **2020**, *8*, 1138. [CrossRef]
13. Chaudhary, R.; Fabbri, P.; Leoni, E.; Mazzanti, F.; Akbari, R.; Antonini, C. Additive Manufacturing by Digital Light Processing: A Review. *Prog. Addit. Manuf.* **2023**, *8*, 331–351. [CrossRef]
14. Zhang, J.; Hu, Q.; Wang, S.; Tao, J.; Gou, M. Digital Light Processing Based Three-Dimensional Printing for Medical Applications. *IJB* **2019**, *6*, 242. [CrossRef] [PubMed]
15. Nam, J.; Kim, M. Advances in Materials and Technologies for Digital Light Processing 3D Printing. *Nano Converg.* **2024**, *11*, 45. [CrossRef] [PubMed]
16. Wang, H.; Zhang, W.; Ladika, D.; Yu, H.; Gailevičius, D.; Wang, H.; Pan, C.; Nair, P.N.S.; Ke, Y.; Mori, T.; et al. Two-Photon Polymerization Lithography for Optics and Photonics: Fundamentals, Materials, Technologies, and Applications. *Adv. Funct. Mater.* **2023**, *33*, 2214211. [CrossRef]
17. Lee, K.-S.; Kim, R.H.; Yang, D.-Y.; Park, S.H. Advances in 3D Nano/Microfabrication Using Two-Photon Initiated Polymerization. *Prog. Polym. Sci.* **2008**, *33*, 631–681. [CrossRef]
18. Al Rashid, A.; Ahmed, W.; Khalid, M.Y.; Koç, M. Vat Photopolymerization of Polymers and Polymer Composites: Processes and Applications. *Addit. Manuf.* **2021**, *47*, 102279. [CrossRef]
19. Kafle, A.; Luis, E.; Silwal, R.; Pan, H.M.; Shrestha, P.L.; Bastola, A.K. 3D/4D Printing of Polymers: Fused Deposition Modelling (FDM), Selective Laser Sintering (SLS), and Stereolithography (SLA). *Polymers* **2021**, *13*, 3101. [CrossRef] [PubMed]

20. Bongiovanni, R.; Vitale, A. Vat Photopolymerization. In *High Resolution Manufacturing from 2D to 3D/4D Printing*; Springer International Publishing: Cham, Switzerland, 2022; pp. 17–46, ISBN 978-3-031-13778-5.
21. Mo, X.; Ouyang, L.; Xiong, Z.; Zhang, T. Advances in Digital Light Processing of Hydrogels. *Biomed. Mater.* **2022**, *17*, 042002. [CrossRef] [PubMed]
22. Graça, A.; Bom, S.; Martins, A.M.; Ribeiro, H.M.; Marto, J. Vat-Based Photopolymerization 3D Printing: From Materials to Topical and Transdermal Applications. *Asian J. Pharm. Sci.* **2024**, *19*, 100940. [CrossRef] [PubMed]
23. Pagac, M.; Hajnys, J.; Ma, Q.-P.; Jancar, L.; Jansa, J.; Stefek, P.; Mesicek, J. A Review of Vat Photopolymerization Technology: Materials, Applications, Challenges, and Future Trends of 3D Printing. *Polymers* **2021**, *13*, 598. [CrossRef] [PubMed]
24. Wang, X.; Liu, J.; Zhang, Y.; Kristiansen, P.M.; Islam, A.; Gilchrist, M.; Zhang, N. Advances in Precision Microfabrication through Digital Light Processing: System Development, Material and Applications. *Virtual Phys. Prototyp.* **2023**, *18*, e2248101. [CrossRef]
25. Ma, Y.; Wang, S.; Wu, Z.-S. Photolithographic Microfabrication of Microbatteries for On-Chip Energy Storage. *Nano-Micro Lett.* **2025**, *17*, 105. [CrossRef] [PubMed]
26. Golhin, A.P.; Tonello, R.; Frisvad, J.R.; Grammatikos, S.; Strandlie, A. Surface Roughness of As-Printed Polymers: A Comprehensive Review. *Int. J. Adv. Manuf. Technol.* **2023**, *127*, 987–1043. [CrossRef]
27. Li, J.; Boyer, C.; Zhang, X. 3D Printing Based on Photopolymerization and Photocatalysts: Review and Prospect. *Macromol. Mater. Eng.* **2022**, *307*, 2200010. [CrossRef]
28. Tao, R.; Gu, Y.; Du, Z.; Lyu, X.; Li, J. Advanced Electrode Processing for Lithium-Ion Battery Manufacturing. *Nat. Rev. Clean Technol.* **2025**, *1*, 116–131. [CrossRef]
29. Yin, G. Advancements in Insulation Technologies for Electric Vehicle Battery Cells—A Review. *IEEE Trans. Dielect. Electr. Insul.* **2025**. [CrossRef]
30. Somers, P.; Münchinger, A.; Maruo, S.; Moser, C.; Xu, X.; Wegener, M. The Physics of 3D Printing with Light. *Nat. Rev. Phys.* **2023**, *6*, 99–113. [CrossRef]
31. Topa-Skwarczyńska, M.; Ortyl, J. Photopolymerization Shrinkage: Strategies for Reduction, Measurement Methods and Future Insights. *Polym. Chem.* **2023**, *14*, 2145–2158. [CrossRef]
32. Baumers, M.; Wildman, R.; Tuck, C.; Dickens, P.; Hague, R. Modeling Build Time, Process Energy Consumption and Cost of Material Jetting-Based Additive Manufacturing. *Print Fabr.* **2015**, *31*, 311–316. [CrossRef] [PubMed]
33. Sartini, M.; Favi, C.; Mandolini, M. Rapid Investment Casting: A Techno-Economic Analysis for Evaluating VAT Photopolymerisation Processes. *Int. J. Adv. Manuf. Technol.* **2024**, *134*, 5717–5739. [CrossRef]
34. Medellin, A.; Du, W.; Miao, G.; Zou, J.; Pei, Z.; Ma, C. Vat Photopolymerization 3D Printing of Nanocomposites: A Literature Review. *J. Micro Nano-Manuf.* **2019**, *7*, 031006. [CrossRef]
35. Lyu, Z.; Lim, G.J.H.; Koh, J.J.; Li, Y.; Ma, Y.; Ding, J.; Wang, J.; Hu, Z.; Wang, J.; Chen, W.; et al. Design and Manufacture of 3D-Printed Batteries. *Joule* **2021**, *5*, 89–114. [CrossRef]
36. Subedi, S.; Liu, S.; Wang, W.; Naser Shovon, S.M.A.; Chen, X.; Ware, H.O.T. Multi-Material Vat Photopolymerization 3D Printing: A Review of Mechanisms and Applications. *npj Adv. Manuf.* **2024**, *1*, 9. [CrossRef]
37. Wang, S.-H.; Kuo, P.-L.; Hsieh, C.-T.; Teng, H. Design of Poly(Acrylonitrile)-Based Gel Electrolytes for High-Performance Lithium Ion Batteries. *ACS Appl. Mater. Interfaces* **2014**, *6*, 19360–19370. [CrossRef] [PubMed]
38. Choi, H.J. Gel Polymer Electrolyte with Improved Adhesion Property Based on Poly(4-Hydroxybutyl Acrylate) for Lithium-Ion Batteries. *Chem. Eng. J.* **2023**, *474*, 145673. [CrossRef]
39. Langevin, S.A.; Tan, B.; Freeman, A.W.; Gagnon, J.C.; Hoffman, C.M.; Logan, M.W.; Maranchi, J.P.; Gerasopoulos, K. UV-Cured Gel Polymer Electrolytes with Improved Stability for Advanced Aqueous Li-Ion Batteries. *Chem. Commun.* **2019**, *55*, 13085–13088. [CrossRef] [PubMed]
40. Zhou, G.; Lin, X.; Liu, J.; Yu, J.; Wu, J.; Law, H.M.; Wang, Z.; Ciucci, F. In Situ Formation of Poly(Butyl Acrylate)-Based Non-Flammable Elastic Quasi-Solid Electrolyte for Dendrite-Free Flexible Lithium Metal Batteries with Long Cycle Life for Wearable Devices. *Energy Storage Mater.* **2021**, *34*, 629–639. [CrossRef]
41. Fan, H.; Li, H.; Fan, L.-Z.; Shi, Q. Preparation and Electrochemical Properties of Gel Polymer Electrolytes Using Triethylene Glycol Diacetate-2-Propenoic Acid Butyl Ester Copolymer for High Energy Density Lithium-Ion Batteries. *J. Power Sources* **2014**, *249*, 392–396. [CrossRef]
42. Kim, Y. The Effect of Plasticizers on Transport and Electrochemical Properties of PEO-Based Electrolytes for Lithium Rechargeable Batteries. *Solid State Ion.* **2002**, *149*, 29–37. [CrossRef]
43. Ha, H.-J.; Kwon, Y.H.; Kim, J.Y.; Lee, S.-Y. A Self-Standing, UV-Cured Polymer Networks-Reinforced Plastic Crystal Composite Electrolyte for a Lithium-Ion Battery. *Electrochim. Acta* **2011**, *57*, 40–45. [CrossRef]
44. He, R.; Echeverri, M.; Ward, D.; Zhu, Y.; Kyu, T. Highly Conductive Solvent-Free Polymer Electrolyte Membrane for Lithium-Ion Batteries: Effect of Prepolymer Molecular Weight. *J. Membr. Sci.* **2016**, *498*, 208–217. [CrossRef]

45. Feng, C.; Kyu, T. Role of Dinitrile Plasticizer Chain Lengths in Electrochemical Performance of Highly Conductive Polymer Electrolyte Membrane for Lithium Ion Battery. *Electrochim. Acta* **2020**, *330*, 135320. [CrossRef]
46. Qi, S.; Li, S.; Zou, W.; Zhang, W.; Wang, X.; Du, L.; Liu, S.; Zhao, J. Enabling Scalable Polymer Electrolyte with Synergetic Ion Conductive Channels via a Two Stage Rheology Tuning UV Polymerization Strategy. *Small* **2022**, *18*, 2202013. [CrossRef] [PubMed]
47. Yuan, B.; Zhao, B.; Wang, Q.; Bai, Y.; Cheng, Z.; Cong, Z.; Lu, Y.; Ji, F.; Shen, F.; Wang, P.-F.; et al. A Thin Composite Polymer Electrolyte with High Room-Temperature Conductivity Enables Mass Production for Solid-State Lithium-Metal Batteries. *Energy Storage Mater.* **2022**, *47*, 288–296. [CrossRef]
48. Wu, Y.; Li, Y.; Wang, Y.; Liu, Q.; Chen, Q.; Chen, M. Advances and Prospects of PVDF Based Polymer Electrolytes. *J. Energy Chem.* **2022**, *64*, 62–84. [CrossRef]
49. Song, M.-K.; Cho, J.-Y.; Cho, B.W.; Rhee, H.-W. Characterization of UV-Cured Gel Polymer Electrolytes for Rechargeable Lithium Batteries. *J. Power Sources* **2002**, *110*, 209–215. [CrossRef]
50. Çakmakçı, E.; Uğur, M.H.; Güngör, A. UV-Cured Polypropylene Mesh-Reinforced Composite Polymer Electrolyte Membranes. *e-Polymers* **2015**, *15*, 103–110. [CrossRef]
51. Kim, J.I.; Choi, Y.G.; Ahn, Y.; Kim, D.; Park, J.H. Optimized Ion-Conductive Pathway in UV-Cured Solid Polymer Electrolytes for All-Solid Lithium/Sodium Ion Batteries. *J. Membr. Sci.* **2021**, *619*, 118771. [CrossRef]
52. Stepniak, I. Compatibility of Poly(bisAEA4)-LiTFSI–MPPipTFSI Ionic Liquid Gel Polymer Electrolyte with Li 4 Ti 5 O 12 Lithium Ion Battery Anode. *J. Power Sources* **2014**, *247*, 112–116. [CrossRef]
53. Stepniak, I.; Andrzejewska, E.; Dembna, A.; Galinski, M. Characterization and Application of N-Methyl-N-Propylpiperidinium Bis(Trifluoromethanesulfonyl)Imide Ionic Liquid–Based Gel Polymer Electrolyte Prepared in Situ by Photopolymerization Method in Lithium Ion Batteries. *Electrochim. Acta* **2014**, *121*, 27–33. [CrossRef]
54. Porthault, H.; Piana, G.; Cesbron, M.; Armel, V.; Bazin, A.; Franger, S.; Oukassi, S. Photo-Initiated Cross-Linking of a Methacrylate/Ionic Liquid Based Gel Polymer Electrolyte: Effect of the Curing Sequence on the Electrochemical Properties. *J. Phys. Chem. C* **2019**, *123*, 18171–18179. [CrossRef]
55. Lee, K.; Shang, Y.; Bobrin, V.A.; Kuchel, R.; Kundu, D.; Corrigan, N.; Boyer, C. 3D Printing Nanostructured Solid Polymer Electrolytes with High Modulus and Conductivity. *Adv. Mater.* **2022**, *34*, 2204816. [CrossRef] [PubMed]
56. Siddiquee, Z.; Lee, H.; Xu, W.; Kyu, T.; Jákli, A. Plasticized Ionic Liquid Crystal Elastomer Emulsion-Based Polymer Electrolyte for Lithium-Ion Batteries. *Batteries* **2025**, *11*, 106. [CrossRef]
57. Lu, F.; Gao, X.; Wu, A.; Sun, N.; Shi, L.; Zheng, L. Lithium-Containing Zwitterionic Poly(Ionic Liquid)s as Polymer Electrolytes for Lithium-Ion Batteries. *J. Phys. Chem. C* **2017**, *121*, 17756–17763. [CrossRef]
58. Trigo López, M.; Reglero Ruiz, J.A.; Pablos, J.L.; Ciurduc, D.E.; Corrales, T.; García, F.C.; García, J.M. Photopolymerization of Ionic Liquids in Flexible Microporous Aramids for Ion Conductive Solid Polyelectrolytes. *J. Photochem. Photobiol. A Chem.* **2022**, *422*, 113571. [CrossRef]
59. Yu, Y.; Lu, F.; Sun, N.; Wu, A.; Pan, W.; Zheng, L. Single Lithium-Ion Polymer Electrolytes Based on Poly(Ionic Liquid)s for Lithium-Ion Batteries. *Soft Matter* **2018**, *14*, 6313–6319. [CrossRef] [PubMed]
60. Jiang, J.; Pan, H.; Lin, W.; Tu, W.; Zhang, H. UV-Induced Semi-Interpenetrating Polymer Electrolyte Membrane for Elevated-Temperature All-Solid-State Lithium-Ion Batteries. *Mater. Chem. Phys.* **2019**, *236*, 121781. [CrossRef]
61. Guan, T.; Rong, Z.; Cheng, F.; Zhang, W.; Chen, J. UV-Cured Interpenetrating Networks of Single-Ion Conducting Polymer Electrolytes for Rechargeable Lithium Metal Batteries. *ACS Appl. Energy Mater.* **2020**, *3*, 12532–12539. [CrossRef]
62. Sutton, P.; Airoldi, M.; Porcarelli, L.; Olmedo-Martínez, J.L.; Mugemana, C.; Bruns, N.; Mecerreyes, D.; Steiner, U.; Gunkel, I. Tuning the Properties of a UV-Polymerized, Cross-Linked Solid Polymer Electrolyte for Lithium Batteries. *Polymers* **2020**, *12*, 595. [CrossRef] [PubMed]
63. Zuo, C.; Zhou, B.; Jo, Y.H.; Li, S.; Chen, G.; Li, S.; Luo, W.; He, D.; Zhou, X.; Xue, Z. Facile Fabrication of a Hybrid Polymer Electrolyte via Initiator-Free Thiol–Ene Photopolymerization for High-Performance All-Solid-State Lithium Metal Batteries. *Polym. Chem.* **2020**, *11*, 2732–2739. [CrossRef]
64. Zuo, C.; Chen, G.; Zhang, Y.; Gan, H.; Li, S.; Yu, L.; Zhou, X.; Xie, X.; Xue, Z. Poly(ε-Caprolactone)-Block-Poly(Ethylene Glycol)-Block-Poly(ε-Caprolactone)-Based Hybrid Polymer Electrolyte for Lithium Metal Batteries. *J. Membr. Sci.* **2020**, *607*, 118132. [CrossRef]
65. Hu, J.; Wang, W.; Peng, H.; Guo, M.; Feng, Y.; Xue, Z.; Ye, Y.; Xie, X. Flexible Organic–Inorganic Hybrid Solid Electrolytes Formed via Thiol–Acrylate Photopolymerization. *Macromolecules* **2017**, *50*, 1970–1980. [CrossRef]
66. Lv, F.; Liu, K.; Wang, Z.; Zhu, J.; Zhao, Y.; Yuan, S. Ultraviolet-Cured Polyethylene Oxide-Based Composite Electrolyte Enabling Stable Cycling of Lithium Battery at Low Temperature. *J. Colloid Interface Sci.* **2021**, *596*, 257–266. [CrossRef] [PubMed]

67. Choi, H.M.; Jun, S.J.; Lee, J.; Ryu, M.-H.; Shin, H.; Jung, K.-N. UV-Cured Polymer Solid Electrolyte Reinforced Using a Ceramic-Polymer Composite Layer for Stable Solid-State Li Metal Batteries. *J. Electrochem. Sci. Technol.* **2023**, *14*, 85–95. [CrossRef]
68. Karuppiah, D.; Komissarenko, D.; Thakur, T.; Yüzbasi, N.S.; Clemens, F.; Reisacher, E.; Kaya, P.; Pikul, J.; Blugan, G. Vat Photopolymerization of Tantalum-Doped Li_7 La_3 Zr_2 O_{12} Electrolytes: A New Frontier in Solid-State Battery Design. *J. Mater. Chem. A* **2025**, *13*, 387–398. [CrossRef]
69. Wang, Y.; Li, X.; Qin, Y.; Zhang, D.; Song, Z.; Ding, S. Local Electric Field Effect of Montmorillonite in Solid Polymer Electrolytes for Lithium Metal Batteries. *Nano Energy* **2021**, *90*, 106490. [CrossRef]
70. Bae, M.; Ahn, S.; You, S.; Kim, J.; Kim, D.; Kim, H.; Kim, H.-I.; Park, J. Expanded Illite Filler in UV-Curable Polymer Electrolytes for All-Solid-State Li-Ion Batteries. *Coatings* **2024**, *14*, 1158. [CrossRef]
71. Zhu, T.; Hao, X.; Cao, Y.; Li, T.; Li, Y.; Wang, W. Ultraviolet-Cured Heat-Resistant and Stretchable Gel Polymer Electrolytes for Flexible and Safe Semi-Solid Lithium-Ion Batteries. *J. Power Sources* **2024**, *613*, 234944. [CrossRef]
72. Wu, Q.; Yang, Y.; Ma, C.; Chen, Z.; Su, Q.; Zhu, C.; Gao, Y.; Ma, R.; Li, C. Flexible Nanocomposite Polymer Electrolyte Based on UV-Cured Polyurethane Acrylate for Lithium Metal Batteries. *ACS Sustain. Chem. Eng.* **2021**, *9*, 5631–5641. [CrossRef]
73. Wang, S.; Bai, M.; Liu, C.; Li, G.; Lu, X.; Cai, H.; Liu, C.; Lai, W.-Y. Highly Stretchable Multifunctional Polymer Ionic Conductor with High Conductivity Based on Organic-Inorganic Dual Networks. *Chem. Eng. J.* **2022**, *440*, 135824. [CrossRef]
74. Zehbe, K.; Lange, A.; Taubert, A. Stereolithography Provides Access to 3D Printed Ionogels with High Ionic Conductivity. *Energy Fuels* **2019**, *33*, 12885–12893. [CrossRef]
75. Chen, Q.; Xu, R.; He, Z.; Zhao, K.; Pan, L. Printing 3D Gel Polymer Electrolyte in Lithium-Ion Microbattery Using Stereolithography. *J. Electrochem. Soc.* **2017**, *164*, A1852–A1857. [CrossRef]
76. Yu, R.; Li, S.; Chen, G.; Zuo, C.; Zhou, B.; Ni, M.; Peng, H.; Xie, X.; Xue, Z. Monochromatic "Photoinitibitor"-Mediated Holographic Photopolymer Electrolytes for Lithium-Ion Batteries. *Adv. Sci.* **2019**, *6*, 1900205. [CrossRef] [PubMed]
77. He, Y.; Chen, S.; Nie, L.; Sun, Z.; Wu, X.; Liu, W. Stereolithography Three-Dimensional Printing Solid Polymer Electrolytes for All-Solid-State Lithium Metal Batteries. *Nano Lett.* **2020**, *20*, 7136–7143. [CrossRef] [PubMed]
78. Maurel, A.; Fernandez, C.A.; Schiaffino, E.M.; Mahmud, M.S.; Delgado Ramos, K.L.; Lin, Y.; MacDonald, E.; Merrill, L.C.; Cardenas, J.A.; Martinez, A.C. Vat Photopolymerization Three-Dimensional Printing of PEGDA/$LiClO_4$ Solid Polymer Electrolytes with Optimised Accuracy and Electrochemical-Mechanical Performance. *Virtual Phys. Prototyp.* **2025**, *20*, e2499480. [CrossRef]
79. Martinez, A.C.; Schiaffino, E.M.; Aranzola, A.P.; Fernandez, C.A.; Seol, M.-L.; Sherrard, C.G.; Jones, J.; Huddleston, W.H.; Dornbusch, D.A.; Sreenivasan, S.T.; et al. Multiprocess 3D Printing of Sodium-Ion Batteries via Vat Photopolymerization and Direct Ink Writing. *J. Phys. Energy* **2023**, *5*, 045010. [CrossRef]
80. Rahman, M.S.; Shiblee, M.N.I.; Ahmed, K.; Khosla, A.; Ogawa, J.; Kawakami, M.; Furukawa, H. Flexible and Conductive 3D Printable Polyvinylidene Fluoride and Poly(*N*, *N*-dimethylacrylamide) Based Gel Polymer Electrolytes. *Macromol. Mater. Eng.* **2020**, *305*, 2000262. [CrossRef]
81. Norjeli, M.F.; Tamchek, N.; Osman, Z.; Mohd Noor, I.S.; Kufian, M.Z.; Ghazali, M.I.B.M. Additive Manufacturing Polyurethane Acrylate via Stereolithography for 3D Structure Polymer Electrolyte Application. *Gels* **2022**, *8*, 589. [CrossRef] [PubMed]
82. Zekoll, S.; Marriner-Edwards, C.; Hekselman, A.K.O.; Kasemchainan, J.; Kuss, C.; Armstrong, D.E.J.; Cai, D.; Wallace, R.J.; Richter, F.H.; Thijssen, J.H.J.; et al. Hybrid Electrolytes with 3D Bicontinuous Ordered Ceramic and Polymer Microchannels for All-Solid-State Batteries. *Energy Environ. Sci.* **2018**, *11*, 185–201. [CrossRef]
83. Vijayakumar, V. In Situ Polymerization Process: An Essential Design Tool for Lithium Polymer Batteries. *Energy Environ. Sci.* **2021**, *14*, 2708–2788. [CrossRef]
84. Yuan, J.; Dong, R.; Li, Y.; Liu, Y.; Zheng, Z.; Liu, Y.; Sun, Y.; Zhong, B.; Wu, Z.; Guo, X. An Integrated Cathode and Solid Electrolyte via in Situ Polymerization with Significantly Reduced Interface Resistance. *Chem. Commun.* **2021**, *57*, 13004–13007. [CrossRef] [PubMed]
85. Lin, K.; Yang, S.; Shi, Z.; Fan, Q.; Liu, Z.; Liu, L. Knitting a Sweater with UV-Induced in Situ Polymerization of Poly(Pyrrole-Co-Citral Nitrile) on Ni-Rich Layer Oxide Cathode Materials for Lithium Ion Batteries. *J. Power Sources* **2022**, *520*, 230768. [CrossRef]
86. Cui, M.; Sun, H.; Xue, Z.; Li, Q.; Zhang, T.; Kang, Q. A PVDF-HFP-Based Gel Polymer Electrolyte onto Air Cathode by UV-Curing for Lithium–Oxygen Batteries. *ACS Appl. Energy Mater.* **2024**, *7*, 11233–11239. [CrossRef]
87. Nara, H.; Yokoshima, T.; Mikuriya, H.; Tsuda, S.; Momma, T.; Osaka, T. The Potential for the Creation of a High Areal Capacity Lithium-Sulfur Battery Using a Metal Foam Current Collector. *J. Electrochem. Soc.* **2017**, *164*, A5026–A5030. [CrossRef]
88. Ahn, S.; Mikuriya, H.; Kojima, E.; Osaka, T. Synthesis of Li Conductive Polymer Layer on 3D Structured S Cathode by Photo-Polymerization for Li–S Batteries. *J. Electrochem. Soc.* **2022**, *169*, 030546. [CrossRef]
89. Xie, C.; Rong, M.; Guo, Q.; Wei, Z.; Chen, Z.; Huang, Q.; Zheng, Z. UV-Permeable 3D Li Anodes for In Situ Fabrication of Interface-Gapless Flexible Solid-State Lithium Metal Batteries. *Adv. Mater.* **2024**, *36*, 2406368. [CrossRef] [PubMed]

90. Zhang, S.S.; Jow, T.R.; Amine, K.; Henriksen, G.L. LiPF6–EC–EMC Electrolyte for Li-Ion Battery. *J. Power Sources* **2002**, *107*, 18–23. [CrossRef]
91. Sheidaei, A.; Xiao, X.; Huang, X.; Hitt, J. Mechanical Behavior of a Battery Separator in Electrolyte Solutions. *J. Power Sources* **2011**, *196*, 8728–8734. [CrossRef]
92. Chan, P.K.; Rey, A.D. Polymerization-Induced Phase Separation. 1. Droplet Size Selection Mechanism. *Macromolecules* **1996**, *29*, 8934–8941. [CrossRef]
93. Chan, P.K.; Rey, A.D. Polymerization-Induced Phase Separation. 2. Morphological Analysis. *Macromolecules* **1997**, *30*, 2135–2143. [CrossRef]
94. Dong, Z.; Cui, H.; Zhang, H.; Wang, F.; Zhan, X.; Mayer, F.; Nestler, B.; Wegener, M.; Levkin, P.A. 3D Printing of Inherently Nanoporous Polymers via Polymerization-Induced Phase Separation. *Nat. Commun.* **2021**, *12*, 247. [CrossRef] [PubMed]
95. Deore, B.; Sampson, K.L.; Lacelle, T.; Kredentser, N.; Lefebvre, J.; Young, L.S.; Hyland, J.; Amaya, R.E.; Tanha, J.; Malenfant, P.R.L.; et al. Direct Printing of Functional 3D Objects Using Polymerization-Induced Phase Separation. *Nat. Commun.* **2021**, *12*, 55. [CrossRef] [PubMed]
96. Ihrner, N.; Johannisson, W.; Sieland, F.; Zenkert, D.; Johansson, M. Structural Lithium Ion Battery Electrolytes via Reaction Induced Phase-Separation. *J. Mater. Chem. A* **2017**, *5*, 25652–25659. [CrossRef]
97. Emilsson, S.; Lindbergh, G.; Johansson, M. Tuneable and Efficient Manufacturing of Li-Ion Battery Separators Using Photopolymerization-Induced Phase Separation. *J. Mater. Chem. A* **2024**, *12*, 30442–30453. [CrossRef]
98. Manly, A.J.; Tenhaeff, W.E. One-Step Fabrication of Robust Lithium Ion Battery Separators by Polymerization-Induced Phase Separation. *J. Mater. Chem. A* **2022**, *10*, 10557–10568. [CrossRef]
99. Manly, A.J.; Tenhaeff, W.E. Mechanically and Thermally Robust Microporous Copolymer Separators for Lithium Ion Batteries. *Electrochim. Acta* **2022**, *425*, 140705. [CrossRef]
100. Maurel, A.; Martinez, A.C.; Grugeon, S.; Panier, S.; Dupont, L.; Cortes, P.; Sherrard, C.G.; Small, I.; Sreenivasan, S.T.; Macdonald, E. Toward High Resolution 3D Printing of Shape-Conformable Batteries via Vat Photopolymerization: Review and Perspective. *IEEE Access* **2021**, *9*, 140654–140666. [CrossRef]
101. Wang, C.; Taherabadi, L.; Jia, G.; Madou, M.; Yeh, Y.; Dunn, B. C-MEMS for the Manufacture of 3D Microbatteries. *Electrochem. Solid-State Lett.* **2004**, *7*, A435. [CrossRef]
102. Narita, K.; Citrin, M.A.; Yang, H.; Xia, X.; Greer, J.R. 3D Architected Carbon Electrodes for Energy Storage. *Adv. Energy Mater.* **2021**, *11*, 2002637. [CrossRef]
103. Wang, M.; Xia, Y.; Wang, X.; Xiao, Y.; Liu, R.; Wu, Q.; Qiu, B.; Metwalli, E.; Xia, S.; Yao, Y.; et al. Silicon Oxycarbide/Carbon Nanohybrids with Tiny Silicon Oxycarbide Particles Embedded in Free Carbon Matrix Based on Photoactive Dental Methacrylates. *ACS Appl. Mater. Interfaces* **2016**, *8*, 13982–13992. [CrossRef]
104. Ali, S.; Jaffer, S.; Maitlo, I.; Shehzad, F.K.; Wang, Q.; Ali, S.; Akram, M.Y.; He, Y.; Nie, J. Photo Cured 3D Porous Silica-Carbon (SiO_2–C) Membrane as Anode Material for High Performance Rechargeable Li-Ion Batteries. *J. Alloys Compd.* **2020**, *812*, 152127. [CrossRef]
105. Ding, S.; Cheng, W.; Zhang, L.; Du, G.; Hao, X.; Nie, G.; Xu, B.; Zhang, M.; Su, Q.; Serra, C.A. Organic Molecule Confinement Reaction for Preparation of the Sn Nanoparticles@graphene Anode Materials in Lithium-Ion Battery. *J. Colloid Interface Sci.* **2021**, *589*, 308–317. [CrossRef] [PubMed]
106. Wang, X.; Cheng, Y.-J.; Ji, Q.; Liang, S.; Ma, L.; Xu, Z.; Zuo, X.; Meng, J.-Q.; Zhu, J.; Müller-Buschbaum, P.; et al. In Situ Incorporation of Super-Small Metallic High Capacity Nanoparticles and Mesoporous Structures for High-Performance TiO_2/SnO_2/Sn/Carbon Nanohybrid Lithium-Ion Battery Anodes. *Energy Technol.* **2020**, *8*, 2000034. [CrossRef]
107. Maurel, A.; Martinez, A.C.; Chavari, S.B.; Yelamanchi, B.; Seol, M.-L.; Dornbusch, D.A.; Huddleston, W.H.; Sreenivasan, S.T.; Sherrard, C.G.; MacDonald, E.; et al. 3D Printed TiO_2 Negative Electrodes for Sodium-Ion and Lithium-Ion Batteries Using Vat Photopolymerization. *J. Electrochem. Soc.* **2023**, *170*, 100538. [CrossRef]
108. Martinez, A.C.; Aranzola, A.P.; Schiaffino, E.; MacDonald, E.; Maurel, A. Additive Manufacturing of $LiCoO_2$ Electrodes via Vat Photopolymerization for Lithium Ion Batteries. *Energy Adv.* **2024**, *3*, 1009–1018. [CrossRef]
109. Yee, D.W.; Citrin, M.A.; Taylor, Z.W.; Saccone, M.A.; Tovmasyan, V.L.; Greer, J.R. Hydrogel-Based Additive Manufacturing of Lithium Cobalt Oxide. *Adv. Mater. Technol.* **2021**, *6*, 2000791. [CrossRef] [PubMed]
110. Martinez, A.C.; Maurel, A.; Aranzola, A.P.; Grugeon, S.; Panier, S.; Dupont, L.; Hernandez-Viezcas, J.A.; Mummareddy, B.; Armstrong, B.L.; Cortes, P.; et al. Additive Manufacturing of LiNi1/3Mn1/3Co1/3O2 Battery Electrode Material via Vat Photopolymerization Precursor Approach. *Sci. Rep.* **2022**, *12*, 19010. [CrossRef] [PubMed]
111. Saccone, M.A.; Greer, J.R. Understanding and Mitigating Mechanical Degradation in Lithium–Sulfur Batteries: Additive Manufacturing of Li2S Composites and Nanomechanical Particle Compressions. *J. Mater. Res.* **2021**, *36*, 3656–3666. [CrossRef]
112. Gulzar, U.; Egorov, V.; Zhang, Y.; O'Dwyer, C. Recyclable 3D-Printed Aqueous Lithium-Ion Battery. *Adv. Energy Sustain. Res.* **2023**, *4*, 2300029. [CrossRef]

113. Cohen, E.; Menkin, S.; Lifshits, M.; Kamir, Y.; Gladkich, A.; Kosa, G.; Golodnitsky, D. Novel Rechargeable 3D-Microbatteries on 3D-Printed-Polymer Substrates: Feasibility Study. *Electrochim. Acta* **2018**, *265*, 690–701. [CrossRef]
114. Martinez, A.C.; Maurel, A.; Yelamanchi, B.; Talin, A.A.; Grugeon, S.; Panier, S.; Dupont, L.; Aranzola, A.; Schiaffino, E.; Sreenivasan, S.T.; et al. Combining 3D Printing of Copper Current Collectors and Electrophoretic Deposition of Electrode Materials for Structural Lithium-Ion Batteries. *Adv. Manuf.* **2025**, *13*, 462–475. [CrossRef]